A Cross-Bridge Cycle with Two Tension-Generating Steps Simulates Skeletal Muscle Mechanics

Gerald Offer and K. W. Ranatunga

Muscle Contraction Group, School of Physiology and Pharmacology, University of Bristol, Bristol, United Kingdom

Supporting Material

1. derivation of strain-dependence of attachment and detachment of pre-tensing heads

The energy of the transition state for detachment of a pre-tensing head from actin is lowered by the application of force F at an angle θ to the direction of the detachment trajectory by a work term $Fd\cos\theta$ where d is the distance moved along this trajectory to reach the transition state (1). This work term increases the rate of detachment by a factor $\exp[Fd\cos\theta/k_BT]$. A force applied along the detachment trajectory (ie at θ=0) would therefore maximally increase the rate of detachment, a force in the opposite direction would maximally inhibit the rate of detachment, and a force perpendicular to the detachment trajectory would not affect the rate. In our case the force is axial and not constant because it is applied by the spring of the crossbridge compliant element. The strain in the spring changes as the myosin head moves away from the actin subunit. If the head is attached to an actin subunit at axial position x, the energy stored in the spring is $\kappa x^2/2$. If the detachment trajectory lies at an angle θ to the positive x axis, at the transition state the strain will be $(x + d\cos\theta)$ and the energy stored in the spring will then be $\kappa(x + d\cos\theta)^2/2$. Hence the energy required to attain the transition state will be increased by the difference, $\kappa d\cos\theta(2x + d\cos\theta)/2$. The rate constant of detachment at x for angle θ, $k_d^{x,\theta}$, is therefore

$k_d^{x,\theta} = k_d^{AM} \exp[-\kappa d\cos\theta(2x + d\cos\theta)/2k_BT]$ ...(S1)

where k_d^{AM} is the rate constant for actomyosin in solution.

Initially, we used a polar mode (Fig. S1a) in which detachment occurred only in the negative x direction ie at $\theta = \pi$. Positive strain in the compliant element therefore enhances, while negative strain inhibits, detachment. For this polar mode the rate constant of detachment at x, k_d^x, is related to that for actomyosin in solution, k_d^{AM}, by

$k_d^x = k_d^{AM} \exp[\kappa d(2x - d)/2k_BT]$ ...(S2)

k_d^x thus increases exponentially with x and becomes small at negative x. The rate constant, k_a^x, for attachment at x for this polar mode can be obtained from this rate constant of detachment and the equilibrium constant for attachment at x.

$k_a^x = k_a^{AM} \exp[-\kappa(x - d)^2/2k_BT]$ ...(S3)

Hence, the dependence of k_a^x on x is Gaussian with a maximum at x=d. This mode of attachment is ratchet-like and would contribute a small amount to tension.

We later used a symmetric mode of detachment (Fig. S1b,c), in which a head can detach from actin along *many* directions away from the actin filament (2). Specifically, we supposed that the direction vectors trace out a hemisphere around the point of attachment of the head to actin such that all θ between 0 and $\theta = \pi$ are possible. In solution, detachment at any of these angles is taken to be equally likely (Fig. S1b), but in muscle the strain in the crossbridge compliant element favours directions where x decreases on detachment (Fig. S1c). Positive strain in the compliant element maximally enhances the rate constant for detachment along the negative x direction, and maximally inhibits detachment along the positive x direction. For negative strain this pattern will be reversed. For detachment along a direction perpendicular to the x axis the rate constant will be the same as in solution, regardless of the strain. For the symmetric mode the rate constant for detachment at x is obtained by averaging the rate constants for all directions. The direction vectors lying between θ and θ+dθ trace out a semi-circular strip of radius $\sin\theta$, semi-circumference $\pi\sin\theta$ and width dθ. So the area of the strip is $\pi\sin\theta$dθ. This compares with the area 2π of the hemispherical surface traced out by all the direction vectors. So the fraction of the direction vectors which have angles between θ and θ+dθ is $\sin\theta$d$\theta/2$. Hence the rate constant for detachment averaged over all directions within the hemisphere is given by

$$k_d^x = \frac{k_d^{AM}}{2}\int_0^{\pi} \exp\left[-\kappa d\cos\theta(2x + d\cos\theta)/2k_BT\right]\sin\theta\, d\theta \quad ...(S4)$$

The rate constant for detachment is at a minimum at x=0 and increases symmetrically as x becomes increasingly positive or negative. The rate constant for attachment at x is similarly

$$k_a^x = \frac{k_a^{AM}}{2}\int_0^{\pi} \exp\left[-\kappa(x + d\cos\theta)^2/2k_BT\right]\sin\theta\, d\theta \quad ...(S5)$$

This is at a maximum at x=0 and decreases symmetrically on either side (see Fig. 1a of main paper).

2. strain dependence of rate constants of forward and reverse tensing step(s)

In their theory to account for the rate of tension recovery after a length step, Huxley and Simmons (3) supposed that a tensing step was a tilting of a rigid head about the actin-myosin interface. They suggested that this rotation might occur in one, or two, or possibly more steps, each (meta)stable intermediate requiring the myosin head and actin subunit to make contact at two sites, while between these positions at only one site. Hence, the energy profile was flat-topped between metastable positions. The energy well for each metastable position was narrow and the edge of each energy well was taken to be a potential transition state. Depending on the strain in the spring, either of these metastable positions could become the effective transition state and this leads to sharp changes in slope of the plot of rate constant versus x. The Huxley-Simmons scheme has been used in modelling (4-6). In this type of scheme only the forward tensing step is strain-sensitive; the reverse step is not. In our case, the tensing step is taken to be a conformational change within the head rather than a tilt about the actin-myosin interface and the energy profile is entirely unknown; so for simplicity we suppose that there is only one transition state for each tensing step and that the strain increases as the conformation in the motor domain changes during the transition.

At the transition state for a tensing step, we took the increase in strain to be a fraction f ($0 \le f \le 1$) of the strain when the conformational change is completed. Hence for a model with a single tensing step with stroke distance l, the spring is stretched by x before the tensing step and is stretched by $x+fl$ at the transition state. Thus the energy of the transition state is enhanced by $\kappa l(2fx + f^2 l)/2$ compared with that before the tensing step. Hence the rate constant for the tensing step at axial position x is given by

$$k_{tens}^x = k_{tens}^{AM} \exp[-\kappa l(2fx + f^2 l)/2k_BT] \quad ...(S6)$$

where k_{tens}^{AM} is the rate constant for the tensing step for actomyosin in solution. So the rate constant for the tensing step decreases exponentially with x. When $x=-fl/2$ the rate constant is the same as in solution. It is much larger than that in solution for more negative x and much smaller for more positive x as is shown in Fig. 1b of the main paper. All this illustrates the effect of tethering of the myosin heads on this rate constant in intact muscle.

The rate constant for the reversal of the tensing step is similarly given by:

$$k_{-tens}^x = k_{-tens}^{AM} \exp[\kappa l(2x - 2fx + l - f^2 l)/2k_BT] \quad ...(S7)$$

At $x=-l(1+f)/2$, it is identical to that in solution. It is smaller at more negative values of x, and larger for higher values, increasing exponentially with x. Note that if $0<f<1$ both the forward tensing step and its reversal are strain-sensitive, unlike the model of Huxley and Simmons (3).

For a model with two tensing steps with stroke distances l_1 and l_2 and f values f_1 and f_2, in Eq. S6 and Eq. S7 l would be replaced by l_1, and f by f_1 for the first tensing step, and x would be replaced by $x+l_1$, l by l_2, and f by f_2 for the second tensing step.

An important question is whether the rate constants of the forward or reverse tensing step are affected by the compliance of the filaments (7,8). In active muscle in the region of filament

overlap, the attached heads crosslink the thick and thin filaments into a three-dimensional network extending across the sarcomere. This means that the filament stiffness that a single head has to work against is very high compared with that of the compliant element of that head. Consequently the extension of the filaments by the execution of a tensing step by a single head is negligible and the above equations will still apply when there is filament compliance. Only after this transition that produces a tiny extra force will mechanical equilibrium be restored by a tiny amount of sliding of the ensemble of thick and thin filaments which slightly reduces the strain of all attached heads (9). Similarly filament compliance will not affect equations for the attachment and detachment of pre-tensing heads.

3. non-Hookean filament stiffness

There is convincing evidence that the stiffness of thick and thin filaments is not Hookean but increases with tension (10-14). Nocella et al. found that the half-sarcomere stiffness was a linear function of the tension increasing by 25% if the tension doubled from its isometric level (14). Thus the half-sarcomere stiffness S at tension P is related to the stiffness S_0 at the isometric tension P_0 by:

$$\frac{S-S_0}{S_0} = 0.25\frac{P-P_0}{P_0} \quad ...(S8)$$

For our modelling we needed to derive the change in filament stiffness as the tension changes. Taking the half-sarcomere compliance to be the sum of the constant compliance contribution by crossbridges and the tension-dependent contribution by the filaments, we obtain for the dependence on tension of the *filament* stiffness F

$$\frac{F}{F_0} = \frac{(1+0.25\frac{P-P_0}{P_0})}{(1-0.25\frac{c}{1-c}\frac{P-P_0}{P_0})} \quad ...(S9)$$

where F_0 is the filament stiffness at the isometric tension and c is the fraction of the half-sarcomere compliance in an isometric contraction contributed by crossbridges. Thus the filament stiffness increases substantially with tension but not in a linear manner. For example with c~0.5, a doubling of the tension from its isometric level would increase the filament stiffness by a factor of 1.67.

4. calculation of occupancies in an isometric contraction

Suppose at any instant of time in an isometric contraction that there are n actin subunits to which a head can bind. Including detached heads, there are a total of N=2n+2 molecular species to be considered for a model with one tensing step, N=3n+2 species for a model with two tensing steps. For each of these molecular species, an equation can be written defining the rate at which the occupancy of that species is changing with time. For example,for a model with one tensing step, the rate of change of occupancy of pre-tensing heads on actin subunit r is given by

$$k_a^r[A]o_{M.ADP.Pi} + k_{rev}^r o_{post}^r - (k_d^r + k_{tens}^r)o_{pre}^r \quad ...(S10)$$

where k_a^r is the bimolecular rate constant for attachment of pre-tensing heads to subunit r, k_d^r is the rate constant of their detachment from subunit r, k_{tens}^r and k_{rev}^r are the rate constants for the tensing step and its reverse on this subunit, [A] is the concentration of free actin, o_{pre}^r and o_{post}^r are the occupancies of pre-tensing and post-tensing heads attached to subunit r, and $o_{M.ADP.Pi}$ is the occupancy of detached primed heads.

An isometric contraction is a true steady state for every myosin head and hence the rate of

change of each of the species is zero. Thus we have a set of N simultaneous equations in the occupancies o_1 to o_N of the (acto)myosin species.

$$\frac{do_1}{dt} = a_{11}o_1 + a_{12}o_2 + a_{13}o_3 + a_{14}o_4 + ... + a_{1N}o_N = 0 \quad ...(S11a)$$

$$\frac{do_N}{dt} = a_{N1}o_1 + a_{N2}o_2 + a_{N3}o_3 + a_{N4}o_4 + ... + a_{NN}o_N = 0 \quad ...(S11b)$$

where the coefficients a_{11}, a_{12}, etc are functions of the solution rate constants and κ, l, d, and f. Redundancy in the equations is avoided by replacing one of the above with an equation which sets the total occupancy of all species to 1.

This set of equations can be considered as a matrix equation $A.o = b$ where A is the matrix of coefficients, namely linear combinations of first-order rate constants etc., and b is the solution vector. These equations were solved computationally by the functions ludcmp and lubksb (15). The rate equations governing the change in occupancy of each species generally contain only first-order rate constants. However, the rate of attachment of a pre-tensing head to the rth actin subunit is given by

$$k_a^r[\mathrm{A}]o_{M.ADP.Pi} = k_a^r[\mathrm{A_{total}}](1-o^r)o_{M.ADP.Pi} \quad ...(S12)$$

where o^r is the occupancy of that actin subunit by myosin heads in all conformations and $[A_{total}]$ is the total actin concentration. Although the set of simultaneous equations is no longer linear, they can be solved iteratively. In the first iteration the free actin concentration was approximated by the total actin concentration. Then the association reactions become pseudo-first-order and the set of simultaneous equations can be solved to obtain an approximate set of occupancies of each of the myosin species. These can be used to calculate the occupancy of each actin subunit to obtain a better solution and further iterations can be used to calculate a more accurate set of occupancies.

5. simplifying assumptions

To keep the models as simple as possible by minimising the number of parameters required for their specification, we made the following assumptions.

(a) There is no competition between different myosin molecules for a given actin subunit. With the high stiffness used in our models, the axial extent of the labelling of an actin filament by a crown of heads is relatively small (see Fig. 1a of main paper) so we do not suppose that there is significant competition between one myosin crown and its neighbours. At each crown there are three myosin molecules but since their origins are 120° apart, again there would be little competition between them.

(b) The two heads of each myosin molecule behave independently of one another. With an occupancy of attached heads in isometric contraction of about 0.5 it is possible that most interactions occur with only one head of each myosin molecule attached but it is of course possible that many of the interactions occur with both heads attached. Indeed, it has been suggested that the increase in fibre stiffness occurring at small lengthening velocities is attributable to recruitment of the second head of each myosin molecule (16,17) although this is contested (14). Dealing with the interactions between the two heads would require several more parameters to be employed to specify a model and at this stage we doubt whether much more insight would be gained.

(c) The compliant elements of the myosin head are Hookean with constant stiffness regardless of the conformation of the attached head and whether the strain is positive or negative. An optical trap study on the stiffness of subfragment-1 attached to actin indicated that over a large range of positive strains (0-7 nm) the stiffness is constant but no measurements were made for negative strains (18). Optical trapping was also used to examine the strain dependence of the stiffness of crossbridges formed between actin and

myosin molecules embedded in myosin-rod cofilaments either in ADP or in the absence of nucleotide (19). When the axial displacement between the actin filament and an attached myosin molecule was altered, the force-displacement plot showed non-linear elasticity. At positive displacements the stiffness was constant. The high stiffnesses found, 2.6 pN/nm in the presence of ADP and 2.9 pN/nm in the absence of nucleotide, are appropriate for two-headed attachment. In contrast the stiffness became very low for negative displacements (0 to -80 nm). The results were explained by the subfragment-2 region of the myosin tail buckling at small negative strains and bending back along the backbone of the filament at higher negative strains. When fully bent back, the heads were able to resist further movement with a stiffness similar to that for positive strain. This is a very reasonable explanation since electron micrographs of isolated native thick filaments show subfragment-2 peeling away from the backbone and the heads a considerable distance from the backbone (20). An important question is whether the subfragment-2 of myosin molecules in intact muscle could buckle since the distance between the surfaces of the thick and thin filaments is much smaller than the length of subfragment-2. So the subfragment-2 might be able to bend out only to a small extent. With this constraint, the subfragment-2 might well be able to exert compressive force. This is also suggested by the fact that the plot of T_1 versus length step for our model with constant crossbridge stiffness is a very good fit to the experimental T_1 plot (Fig. 4 of main paper) and both meet the length step axis at an angle (21).

(d) The stroke distance for a tensing step is constant and independent of load and velocity. This is discussed in section 11c.

(e) Tension during both shortening and lengthening is borne solely by crossbridges. There is evidence, particularly during lengthening, that structures other than crossbridges contribute to tension. Thus after the end of a ramp stretch the force declines but to a level higher than the isometric level and this is maintained for hundreds of milliseconds (22). It has been suggested that this residual force enhancement may arise by stretch of titin filaments stiffened by interactions with actin (23,24). Because the nature of the residual force enhancement is still speculative, we did not consider it appropriate to incorporate it into the modelling at this juncture.

6. choice of limits of parameters

The model with one tensing step requires thirteen adjustable parameters to be specified. Seven are required to define the rate constants of the crossbridge cycle in solution. Three define the strain-dependencies of steps in the cycle: attachment/detachment of pre-tensing heads, tensing and detachment of post-tensing heads. The remaining three are mechanical parameters, the stroke distance, the crossbridge stiffness, and the fraction of the half-sarcomere compliance in an isometric contraction due to crossbridges. For the model with a second tensing step, a further four parameters are required; the forward and reverse rate constants of this second step, its strain dependence and its stroke distance. Each of these parameters was allowed to assume a starting value within a range determined partly from literature values and partly from the experience gained from preliminary modelling.

Consider first the parameters for the models with a single tensing step. K'^{AM}_{tens}, the first-order equilibrium constant for the tensing step in solution, is uncertain. Smith and Geeves (4) quote a value of 10^3 for the first-order equilibrium constant of the overall reaction AM.ADP.Pi = AM.ADP + Pi at the cellular concentration of 1 mM Pi. However, a value 100 times higher than this is obtained by combining the equilibrium constant for the dissociation of both products (25) with the equilibrium constant for dissociation of ADP from AM.ADP (4). So for the initial simulated annealing run we allowed K'^{AM}_{tens} to take values in the range 10 to 10^4. k^{AM}_{tens}, the *rate* constant of the tensing step in solution, was initially allowed to assume values

in the range 10^3 to $5x10^4$ s^{-1}. k_d^{AM}, the rate constant for detachment of pre-tensing heads from actin in solution, was initially allowed to take starting values from 10 to 400 s^{-1}. For frog muscle only the lower limit (5 s^{-1}) of $k_{hyd,}$ the rate constant of the ATP hydrolysis step on detached myosin heads, is known (26). For rabbit myosin at 20°C this rate is 100 s^{-1}, and we allowed k_{hyd} to vary between 30 and 250 s^{-1}. The bimolecular rate constant for the attachment of free myosin heads in the pre-tensing conformation to actin in the absence of strain, is about 10^6 $M^{-1}s^{-1}$ (4) and we initially allowed this parameter to take values in the range $2x10^4$ to $4x10^5$ $M^{-1}s^{-1}$. Taking the effective actin concentration to be identical to the total actin concentration in myofibrils, 0.001 M, this is equivalent to a first-order rate constant $k_a^{'AM}$ in the range 20-400 s^{-1}. Our guideline value of k_i^{AM}, the rate constant in solution or in the absence of strain for detachment of post-tensing heads, was 400 s^{-1}, the lower bound for the rate constant of release of ADP in fibres (27) and we initially allowed values in the range 400 to 5000 s^{-1}. The parameter Δ_D, the extra strain required to reach the transition state of the essentially irreversible ADP-release step (4), was initially allowed to fall in the range 0.8 to 3 nm. We initially allowed values of the stroke distance l between 4 and 11 nm. The value of crossbridge stiffness κ for myosin from Rana temporaria is controversial. Huxley and Tideswell (28) considered it to be ~2.0 pN/nm but there have been recent claims that it is as high as 3.3 pN/nm (29). We have recently reassessed this evidence and consider that there is no compelling evidence that the stiffness of frog myosin is higher than of rabbit myosin (1.7 pN/nm) (30). Nevertheless, we initially allowed values in the range 1.2 to 3.5 pN/nm. We initially allowed values of the interaction distance, d, defining the partitioning of the effect of strain on the rate constants of detachment and attachment (31) to be in the range 0.3 to 0.7 nm. To explain the faster rate of early tension recovery reported for releases than stretches (3,21), the parameter f that governs the strain sensitivity of the rate constants for the tensing step and reverse tensing step might have been expected to be greater than 0.5 and values in the range 0.5 to 1 were initially allowed. Finally, to take into account the presence of filament compliance, the parameter c, the fraction of the half-sarcomere compliance in an isometric contraction contributed by crossbridges, was allowed to fall in the range 0.3 to 0.9.

For models with two tensing steps we allowed values for the first-order equilibrium constants for both first and second tensing steps to fall in the range 10 to 10^3 and the rate constants in the range 10^3 to $5x10^4$ s^{-1}. The parameters f_1 and f_2 that govern the relative strain sensitivities of the rate constants for the forward and reverse tensing steps and reverse tensing steps were both initially allowed to lie in the range 0.5 to 1. The other parameters were the same as for the models with one tensing step.

7. change of refinement protocol

We initially carried out simulated annealing refinement of the starting models treating the sites along actin filaments that can bind a myosin head as being linearly disposed at axial intervals of 5.46 nm ie ignoring the helical structure of the actin filament and hence not considering target areas. During each simulated annealing run typically ~10^5 variants of each model were examined and scored.

With increasing experience, the protocol used to refine and score the models against the experimental data evolved. Examining the results of the simulated annealing runs, we noted that those models that had a high equilibrium constant for the binding to actin of pre-tensing heads tended to have a substantially greater optimum thermodynamic efficiency (>30%) than those with a low equilibrium constant (efficiency of 20-25%). But for such models the occupancy of attached heads in an isometric contraction was unrealistically high (>90%). So further repeated downhill simplex refinements now treated the sites along an actin filament to which a myosin head on a neighbouring thick filament can bind as a succession of target

areas each consisting of only three adjacent actin subunits alternating between the two long-pitched helical strands (see Methods). This reduced the occupancy of attached heads but kept the efficiency high.

We also noted that attempting to score models for the T_2 tension values given by a range of length steps was unsatisfactory because, especially in the early stages of a refinement, it was common to find that the features that Ford et al. (21) had used to define the boundary between phases 2 and 3 ie a tension minimum, maximum or inflection, were not present, so that the value of T_2 could not reliably be assessed. A better strategy was therefore to score the models by the entire time course of phases 2, 3 and 4 in addition to the T_1 value (see Methods).

Additionally it was not uncommon during a refinement that one or more of the parameters reached the upper or lower limit of its allowed range. It was therefore necessary, when appropriate, to expand (or sometimes to reduce) the allowed range of that parameter in a subsequent downhill simplex refinement. The final upper and lower limits for the parameter space for the models with one or two tensing steps are shown in Tables S1a and S1b respectively.

The models, especially those with a single tensing step, tended to have too low a crossbridge stiffness. We therefore in later studies included in the scoring a penalty if the stiffness were lower than our target of 1.7 pN/nm, but recognising suggestions that the stiffness may be as high as 3.3 pN/nm (29) we gave no penalty if the crossbridge stiffness were greater than 1.7 pN/nm. This penalty only slightly reduced the fit to the force-velocity relation and transient response to length steps for models with two tensing steps, but adversely affected the fit for models with one tensing step.

Finally, evidence accumulated that the filament stiffness was not constant as we had initially assumed but increased with tension (10-14). We therefore re-refined the earlier Hookean models using downhill simplex runs but now allowing the filament stiffness to vary with tension in the manner described in section 3.

8. interval between intercepts of T_1/T_0 and T_2/T_0 plots

The intercepts (y_1 and y_2) of the plots of T_1/T_0 and T_2/T_0 against length step have previously been interpreted in several different ways to estimate the (total) stroke distance. The plot of T_2/T_0 versus length step is roughly parallel to that for T_1/T_0 for large releases (21,32), indicating that such releases cause the tension to rise in the early tension recovery by a constant $T_0(y_2 - y_1)/y_1$. The simplest interpretation is that such large releases are not accompanied by attachment or detachment of crossbridges but cause *all* the attached heads to reach the post-tensing state. If the occupancies of the pre- and mid-tensing states in an isometric contraction are o_{pre} and o_{mid}, then the tension increase due to the conversion of the pre-tensing heads to the post-tensing state would be $\kappa c o_{pre}(l_1 + l_2)$, where c is the fraction of the half-sarcomere compliance in an isometric contraction due to crossbridges. Similarly, the tension increase due to the conversion of the mid-tensing heads to the post-tensing state would be $\kappa c o_{mid} l_2$. The release of y_1 nm/hs causes the tension to fall concomitantly by T_0 due to the strain in all attached heads falling by cy_1. Hence $T_0/y_1 = \kappa o_{\mathrm{T}}\, c$ where o_{T} is the total occupancy of all attached heads. Thus the interval between the intercepts of the plots of T_1/T_0 and T_2/T_0 against length step is given by

$$y_1 - y_2 = \left(o_{pre}(l_1 + l_2) + o_{mid} l_2\right)/o_T \quad \text{...(S13a)}$$

If there were only one tensing step, this interval simplifies to

$y_1 - y_2 = o_{pre} l / o_T$ ...(S13b).

9. long time-course of tension transients after length steps

Fig. S2 shows over a longer (200 ms) time period the tension transients exhibited by the best model with two tensing steps after a series of releases and a stretch. For the releases (a-c) the tension-time plots resemble the experimental data of Ford et al. (21) fairly closely. However, while the small initial very rapid tension fall following the stretch (d) was similar to the experimental, this fall slows quickly and the model showed no delayed tension rise.

10. tension contribution by attached states

The velocity dependence of the tension contributions of attached heads in each of the three conformations are compared in Fig. S3 for the best model with two tensing steps. In an isometric contraction the heads in the pre-tensing conformation exerted a fraction 34% of the total tension. The tension exerted by such heads increased steeply with velocity around the isometric point and at lengthening velocities greater than 0.003 nm/ms they became the major contributor to tension. Conversely, at *shortening* velocities greater than 0.2 nm/ms these heads contributed <10% of the tension. The tension exerted by heads in the mid-tensing conformation was maximal at a very small shortening velocity (0.013 nm/ms) and decreased slowly with further increase of shortening velocity but steeply with increase of lengthening velocity. The tension contribution of the post-tensing conformation was very small in an isometric contraction or on lengthening but increased with small shortening velocities reaching a maximum at a shortening velocity of 0.2 nm/ms, before declining with further increase in shortening velocity and becoming negative at shortening velocities greater than 1.1 nm/ms. At the velocity of unloaded shortening, the positive tension contributed by the mid-tensing heads matched the negative tension contributed by the post-tensing heads.

11. wider significance of model

A model is the quantitative expression of an hypothesis and as such is open to falsification by experiment or theory. The thinking involved in setting up a model ensures that the hypothesis is as precise as possible, leaving no room for vagueness. As all current models make several simplifying assumptions, they are all likely to be wrong at least in detail, if not in substance. However, a model that proves to be wrong may still be of value in opening up topics that merit further debate, in aiding the interpretation of experiments, in providing insight into problems, and in challenging existing notions. We believe that our model has wider significance in challenging current perceptions discussed below of how the crossbridge cycle works and hence furthering the aim of a better understanding.

(a) degree of cooperativity of crossbridges

For actomyosin in solution the myosin heads are not constrained in their ability to interact with actin by being tethered to the backbone of a thick filament. Heads could therefore interact with actin independently of one another except at high myosin concentrations when they would compete for actin sites. In contrast, in muscle the tethering of the heads of myosin molecules to thick filament backbones would be expected to affect their independence. We shall assume that the motor domain of an attached head does not tilt about its interface with actin. For the purposes of this discussion we shall also assume that the compliance of the head is located at the junction of the converter subdomain with the lever arm (30,33), although the arguments are not much altered if some of the compliance arises by bending of the lever arm. We take the orientation of the converter to be determined by the conformational state of the motor domain. This orientation then dictates the unstrained angle of the lever arm (Fig. S4a). But, depending on the crossbridge compliance, forces applied to the end of the lever arm or thermal energy would cause it to swing on either side of that angle by straining the spring of the converter (Fig. S4b,c). If the crossbridge stiffness were low, the

range of lever arm angles would be large (Fig. S4b), if the stiffness were high, the range would be small (Fig. S4c).

We consider two extremes. If the crossbridge stiffness were very high and the angle of the lever arm were restricted to a narrow range for any one conformational state, the lever arm angle and conformational state would be tightly coupled. Consequently, for the end of the lever arm to swing through its complete range of axial movement (~10 nm), there would need to be many conformational states each associated with a different unstrained lever arm angle i.e. there would be many tensing steps, each of them changing the unstrained lever arm angle by only a small amount, so that the energy required for that step would not be too large. Another consequence of a high crossbridge stiffness would be that heads could attach to an actin subunit only if were axially very close. So when heads attached in the pre-stroke conformation, they would do so with very similar lever arm angles (Fig. S4d). Assuming that to produce isometric tension a small amount of filament sliding occurs, the heads would be in conformations similar to that of their initial attachment and with similar lever arm angles. If as a result of a load or length step, the filaments slid, the angle of the lever arm of all attached heads would change accompanied by a near-synchronous change in conformational state (Fig. S4e). This account has been advocated by the Lombardi-Piazzesi-Irving and H.E. Huxley groups (29,34-37) and we call this a high cooperativity mechanism.

During steady shortening since heads would attach at different times, this near-synchronicity would not occur and there would be a mix of conformations and lever arm angles. But even so, when filaments slide, the origin of each crossbridge, the head-tail junction of the myosin molecule, must move with the thick filament backbone and the lever arms of all attached heads, although they may differ in angle, must swing at the same *rate* regardless of the crossbridge stiffness.

In contrast, at the other extreme, with a very low crossbridge stiffness, the lever arm could assume a wide range of angles without change of conformational state of the motor domain. In other words the lever arm angle would not absolutely determine the conformational state and there would need to be only a few (say two or three) states. Another consequence of low crossbridge stiffness would be that a head could attach to actin subunits over a wider axial range. So when pre-stroke heads attached to actin, their lever arms could adopt a wide range of angles by straining the compliant element (Fig. S4f). And subsequently isometric tension could be produced by only a fraction of the heads undergoing a tensing step (Fig. S4g). Because the heads could change their conformation relatively independently of one another and from filament sliding, we call this a low cooperativity mechanism.

The question is how far along the spectrum between these extremes would be implied by a crossbridge stiffness of 1.7 pN/nm (that of our model) or the higher level of 3.3 pN/nm that has been proposed (29). Suppose the end of the lever arm of a head with thermal energy $k_B T$ is displaced axially from its lowest energy position by x then

$\frac{\kappa}{2} x^2 = k_B T$ where κ is the crossbridge stiffness.

So this thermal energy can move the end of the lever arm by

$$x = \pm\sqrt{\frac{2k_B T}{\kappa}}$$

For T=276K this becomes $x = \pm\frac{2.76}{\sqrt{\kappa}}$

This square root relation suggests that the flexibility of the lever arm is relatively insensitive to κ: eg for the crossbridge stiffness, 1.7 pN/nm, of our model with two tensing steps $x = \pm 2.1$ nm, while for the crossbridge stiffness of 3.3 pN/nm this decreases only to

$x = \pm 1.5$ nm. This suggests that a difference of twofold in κ would not lead to a great change in the flexibility of the lever arm and consequent crosssbridge behaviour but rather the change would be more moderate. This argument suggests that there would need to be three or four conformational states to allow the end of the lever arm to move through 10 nm if the crossbridge stiffness were as high as 3.3 pN/nm but only two or three states if the crossbridge stiffness were 1.7 pN/nm.

Our modelling has shown that with a crossbridge stiffness of 1.7 pN/nm a low-cooperativity mechanism where heads behave largely independently of one another can operate. Fig. 2d of the main paper shows that for our model in an isometric contraction 54.7% of the attached heads are in the pre-tensing state, while 44.5% have undergone the first tensing step. This is very different behaviour from than that proposed by the Lombardi-Piazzesi-Irving and Huxley groups where all attached heads are supposed to be in the same state, or very similar states. Nor in our model do the heads behave synchronously in response to length or load steps. Fig. S5 shows the time course of the occupancies of attached states in response to a length release of 3 nm/hs. The transition between pre- and mid-tensing states, and between mid- and post-tensing states, is smooth and progressive as would be expected of a stochastic process with low cooperativity.

(b) number of tensing steps
Decostre et al. (29) have suggested that because the crossbridge stiffness is high, there must be at least four tensing steps in the crossbridge cycle. This would produce a kinetic mechanism of daunting complexity. To the contrary, the main paper indicates that a mechanism with only two tensing steps suffices to account for the force-velocity relation and transient tension responses to length steps.

(c) the model challenges claims that the stroke distance alters with load
In the past the term stroke distance (or throw) of the crossbridge was used to mean the swing of the crossbridge for a tension-generating step if the head were not tethered to the thick filament backbone such as would occur in solution. For the lever arm mechanism that would mean the axial distance moved by the distal end of the lever arm. It has been claimed from X-ray diffraction experiments that the stroke distance alters with load (34,35). That would be a truism if the stroke distance were re-defined to mean the distance swung by the lever arm while a head was attached. For example, in a steady-state isometric contraction the lever arm cannot swing, so by that new definition the stroke distance would be zero. At the other extreme in an unloaded contraction the lever arm might swing beyond the point when its stored energy had been used to do work so that its tension was negative; in that case the lever arm swing would be large. Our model which has, on the older definition, constant stroke distances for the two tensing steps, gives similar changes of the intensity and interference splitting of the M3 meridional reflection experimentally observed (35). That means that their conclusions that the stroke distance alters with load are not, we think, justified.

(d) the model improves understanding of how muscle can conserve energy in isometrically contracting muscle and have a high thermodynamic efficiency in shortening muscle
As discussed in section 3 of the Discussion of the main paper, our model has a very low turnover rate in isometrically contracting muscle thereby conserving ATP, but can respond very rapidly to length changes. In shortening muscle it shows a high thermodynamic efficiency. Both these properties arise from the steep dependence of the rate constant of the forward tensing steps to strain (Fig. 1a).

(e) the model can resolve the staircase shortening paradox
The view that one turn of the cross-bridge cycle was driven by the hydrolysis of one ATP molecule was challenged by the interpretation given by experiments in which muscle was

allowed to shorten in multiple steps (a "staircase") rather than smoothly (38,39). The response to the first release of the series resembled that for a single length step (3). Concurrent with the release, the tension rapidly fell and then partially recovered due to heads executing the tension-generating step. Remarkably, if releases were given at regular short intervals the tension just before each release was regained by the end of each interval and the pattern of tension change became repetitive. Lombardi et al. (38) drew attention to the paradox that the muscle was able to regenerate itself to execute another tension recovery within ~8 ms, although the turnover of the ATPase cycle was supposed to be much slower. They postulated that, after a tension-generating step, the cross-bridges detach without involvement of ATP, rapidly reattach and execute another tension-generating step and proposed that 1 ATP molecule could fuel as many as three cycles (40). However, Chen & Brenner (41) argued that the regeneration of the ability of the muscle to repeat the tension recovery in a short interval could be explained by rapid redistribution among the crossbridge states through steps other than the slow ATP-induced detachment of post-stroke heads. This is certainly an important part of the explanation. However, an implicit assumption made by Lombardi et al. went largely unchallenged: this was that *all* the attached heads respond to a release by executing a tensing step. They also supposed that the ATPase (turnover) rate was no greater than 6 s^{-1} the experimental rate reported at the time. This would have implied that the efficiency was very large. Because the paradox has been so influential (28,42), we have simulated staircase shortening with our mechano-kinetic model.

The main features of the staircase can be satisfactorily simulated with our model without assuming unusual kinetics (Fig. S6a,b). After the fifth release of 4 nm per half-sarcomere at 8 ms intervals, the transient responses to each release of tension and the occupancies of the five states became repetitive. In this repetitive phase, at the beginning and end of each 8 ms time interval, the tension was 55% of the isometric tension, appropriate for the *average* shortening velocity of 0.5 nm/ms. During each release the tension fell to only 4% of that just before the release but then there was a rapid early tension recovery followed by a slower return to the starting value. The time course of the throughput through the tensing steps, the fraction of all the heads that pass through these steps by a given time, is shown in Fig. S6c. In the first two ms of each 8 ms interval, after a very short lag, there is a burst of throughput through the first tensing step of a fraction of 0.1 of the heads followed by a slower steady near-linear increase totalling a fraction of only 0.13 heads by the end of the 8 ms interval. The burst of the throughput through the second tensing step is slower but again by the end of the interval the total throughput represents a fraction of 0.13 of the heads. The rate of ATP consumption is more nearly constant, but necessarily for a model in which one ATP is consumed per cycle, in each interval the ATP consumed exactly equals the total number of heads executing each of the tensing steps (Fig. S6c). Importantly, the tension recovery after each release in these staircase simulations is thus associated with only 13% of the heads undergoing the tensing steps, rather than a majority doing so as previously implicitly assumed (38). These authors proposed two kinetic schemes to explain their results (40,43). In both, two cyclic pathways operated in parallel and a common feature was the proposed reattachment of heads after strain-induced detachment at a much faster rate than the original attachment.

The regeneration of the ability of the muscle to respond in an identical manner from one release to the next requires the occupancies of all crossbridge states to return to the same level at the end of each interval as at its start (41). That occurs because the net rates of all steps increase substantially from their values in an isometric contraction as a result of the changing cross-bridge strain after each release; hence rapid re-equilibration is possible. The *net* rates of all steps in isometrically contracting muscle are necessarily equal to one another and to the ATPase (turnover) rate (0.37 s^{-1} in our model). In the repetitive phase of the staircase in our model, the net flux through the first tensing step increased from 4.8 s^{-1} at the start of each 8 ms interval, to 450 s^{-1} at the end of the release. The net flux through the second

tensing step increased from 3.1 s^{-1} at the start of each interval, to 240 s^{-1} at the end of the release. This acceleration explains how the tension is recovered on the millisecond time scale. The *net* rate of attachment of pre-tensing heads to actin during the staircase is higher than in an isometric contraction; at the start of each 8 nm interval it was 13 s^{-1} and increased to 23 s^{-1} before declining to the starting value. This explains how the occupancy of pre-stroke heads is regained by the end of the interval. Similarly, the rate of the detachment of post-tensing heads was 8.3 s^{-1} at the beginning of each interval and rose to 26 s^{-1} before declining back to the start. This elevated rate allows the occupancy of the post-tensing heads to return to its starting level by the end of the interval.

In our model, the ATPase (turnover) rate in an isometric contraction was 0.37 s^{-1}. If the average turnover rate during staircase shortening were no higher than 6 s^{-1} as assumed by Lombardi et al. (38) the number of ATP molecules hydrolysed per head in the 8 ms time interval would be only 0.003. This would provide enough energy for the 0.13 heads to execute the tensing steps in this interval only if they were capable of undertaking more than 40 cycles per ATP. However, in our simulations, the turnover rate averaged over each 8 ms interval of the staircase increased greatly to 16 s^{-1}, unsurprisingly very similar to that in our simulations of smooth (unstepped) shortening at the same average velocity. This is consistent with experimental findings that the energy output of muscle undertaking a staircase shortening is similar to that in steady shortening (42). Thus there is no need to suppose that the heads undergo more than one crossbridge cycle for each ATP hydrolysed and the paradox is resolved. There is therefore also no need to embrace the complexity of having two cyclic pathways.

(f) The model gives insight on the drag force and drag distance in shortening muscle
The energy stored in a crossbridge as a result of a tensing step is used to do work on the external load as the filaments slide. If a head detaches before its tension is reduced to zero, this energy is wasted as heat. If it remains attached after the tension is reduced to zero, a negative tension or drag force is produced. The drag distance is the average distance slid by the filaments while a crossbridge is exerting drag force.

At low loads the average distance the filaments slide between successive attachments of a given head can be estimated from the sliding distance per ATP hydrolysed, assuming that 1 ATP is hydrolysed per cycle. Higuchi & Goldman (44) reported that this is at least 40 nm. Taking the stroke distance to be 12 nm, they concluded that the drag distance was the difference between these (28 nm). The difficulty with that interpretation is that if the crossbridge stiffness for negative strains were comparable to that for positive strains, the drag force would become very large before the crossbridges detached. Note however that the sliding distance per ATP hydrolysed may be much larger than the working distance, the distance filaments slide while a head is attached, because a head may spend a substantial time detached while the filaments carry on sliding (45) ie a head after detachment may skip over many actin subunits before having another productive encounter. Since the drag distance is the difference between the *working distance* and the stroke distance, the value of 28 nm is likely to overestimate the drag distance.

Since the working distance and drag distance are hard to measure experimentally, our model may give insights on the number and state of the crossbridges that contribute drag force and over what distance they exert this drag force before detaching. Fig. S7a shows the *strain* (z) distribution of occupancies of heads in the three attached states for the case where the shortening velocity is at a maximum (v_{max} = -1.79 nm/ms) and the total tension is zero. All three states (pre- mid- and post-tensing) contribute negative as well as positive strains; the total positive tension is matched by the total negative tension. For the pre- and mid-tensing heads the distribution is roughly bell-shaped but for the post-tensing heads the distribution

has a long tail on the side of negative strain. 60% of the pre-tensing heads, 19% of the mid-tensing heads and 50% of the post-tensing heads carry negative tension at v_{max}. In the case of the pre-tensing and mid-tensing heads the most negative strain is ~ -3 nm, but for the post-tensing heads the tail of the distribution continues to -24 nm. The *average* strain for those pre-tensing heads that are exerting drag force is -0.9 nm; it is -1.0 nm for mid-tensing heads and -5.1 nm for post-tensing heads. Fig. S7b shows the axial distribution of the flux (rate) of detaching post-stroke at v_{max}. The distribution is very broad indicating that detachment of crossbridges occurs over a very wide range of strains due to its stochastic nature. The distribution is also markedly asymmetrical with the flux falling off steeply on the side of positive strain and much more gradually on the side of negative strain. Many heads detach when their strain is still positive and therefore contribute no drag force at all. Indeed the peak flux actually occurs at a small positive strain (2 nm). Other heads detach when their strain is negative but small, and a decreasing number detach at more negative strains where they exert large drag force. Thus our model presents a picture of the drag force being probabilistic rather than deterministic.

(g) The model accounts for the lag in the rise of crossbridge attachment and tension behind the stiffness increase during activation

Fig. S8 shows a simulation of the time course of the rises of stiffness, occupancy of attached heads and tension during activation. For simplicity, it has been assumed that the thin filament activation increases linearly with time and is complete by 20 ms. The stiffness of the half-sarcomere lags behind the activity of the thin filaments by 2 ms at the midpoint. This occurs because of the time required for heads to attach thus increasing stiffness. In turn, the rise in occupancy of the attached heads lags behind the rise in stiffness by 5 ms. This occurs because the contribution of filaments to sarcomere compliance means that the stiffness is not proportional to the number of attached crossbridges. The rise in tension lags only slightly behind (1.6 ms) the rise in number of attached crossbridges because the first tensing step is so fast.

Thus the lag of the rise of tension behind the rise of stiffness on activation (46-48) is largely due to the contribution made by filaments to the half-sarcomere compliance so that the stiffness is not proportional to crossbridge number. On the previous interpretation this lag was attributed to a slow tensing step.

(h) The model accounts for the increase in fibre stiffness in rapid stretches

It is well established that a rapid stretch causes an increase in fibre stiffness (14,16,17) but there is debate over whether this is due to crossbridge recruitment or whether the filaments show non-Hookean behaviour. Fig. S9 shows a simulation of the time course of tension as a result of a stretch of 50 nm/hs in 0.5 ms which can be compared with figure 1 of Nocella et al. (14). In one run (blue trace) a 4 kHz oscillation with amplitude of 0.5 nm/hs has been superposed; the red trace shows the time course without this oscillation. The green trace giving the difference shows that the half-sarcomere stiffness increases during the stretch itself and at the end of the stretch it has increased 18% compared with the isometric level.

(i) The model accounts for the increase in fibre stiffness at small lengthening velocities without requiring crossbridge recruitment

In steady lengthening the tension nearly doubles accompanied by a small increase in fibre stiffness above the isometric level (49). Both contribute to the braking action. The maximum stiffness increase of ~10-20% is observed at a small lengthening velocity (~ 0.1 nm/ms) and there is no further increase at larger velocities. The large increase of tension during lengthening was initially attributed to pre-stroke heads attaching at low strains and then being dragged to high strains before detaching (49). At that time it was not appreciated that filaments were compliant, and it was supposed that the small increase in stiffness was for

kinetic reasons and there was no increase in the number of attached crossbridges. When it later became clear that filaments were compliant, the increase in fibre stiffness implied that lengthening caused the number of attached heads to double assuming that both crossbridges and filaments were Hookean. The rise in stiffness during lengthening was then attributed to the very rapid attachment to actin of the second head of myosin molecules (16,17).

There have, however, been indications that the filaments are not Hookean and their stiffness increases with tension (10-14). Very recently Nocella et al. (14) have provided convincing evidence that the increase in fibre stiffness during lengthening arises largely from the non-Hookean behaviour of the filaments and our model is based on their conclusion. Fig. S10 shows for our non-Hookean model the velocity dependence of the occupancy of attached heads and the half-sarcomere stiffness. The occupancy of attached heads and the half-sarcomere stiffness declines with increase of shortening velocity and in unloaded shortening falls to 43% and 48% of the isometric level respectively. While for the precursor Hookean model the fall in occupancy was similar (41%), the fall in stiffness was smaller (to 61% of the isometric level). The stiffness of our non-Hookean model increases with small lengthening velocities reaching a maximum 12% higher than the isometric level at a lengthening velocity of 0.05-0.1 nm/ms despite a fall in occupancy of attached heads, whereas the precursor Hookean model showed a continuous fall with lengthening velocity. This supports the view of Nocella et al. (14) that the rise in stiffness, which contributes to the braking action, is not due to recruitment of attached heads but is due to the non-Hookean behaviour of the filaments.

12. Comparison of our model with other models of the crossbridge cycle

In Table S2 our model is compared with a selection of models of the complete crossbridge cycle which have been used to fit the force-velocity relation and/or the tension transients after length steps.

Supporting References

1. Evans, E. 2001. Probing the relation between force-lifetime and chemistry in single molecular bonds. Ann. Rev. Biophys. Biomol. Struct. 30:105-128.
2. Nishizaka, T., H. Miyata, H. Yoshikawa, S. Ishiwata, and K. Kinosita. 1995. Unbinding force of a single motor molecule of muscle measured using optical tweezers. Nature. 377:251-254.
3. Huxley, A.F., and R.M. Simmons. 1971. Proposed mechanism of force generation in striated muscle. Nature. 233:533-538.
4. Smith, D.A., and M.A. Geeves. 1995. Strain-dependent cross-bridge cycle for muscle. Biophys. J. 69:524-537.
5. Smith, D.A., and M.A. Geeves. 1995. Strain-dependent cross-bridge cycle for muscle. II Steady-state behavior. Biophys. J. 69:538-552.
6. Smith, D.A., and J. Sleep. 2004. Mechanokinetics of rapid tension recovery in muscle: the myosin working stroke is followed by a slower release of phosphate. Biophys. J. 87:442-456.
7. Huxley, H.E., S. Stewart, H. Sosa, and T. Irving. 1994. X-ray diffraction measurements of the extensibility of actin and myosin filaments in contracting muscle. Biophys. J. 67:2411-2421.
8. Wakabayashi, K., Y. Sugimoto, H. Tanaka, Y. Ueno, Y. Takezawa, and Y. Amemiya. 1994. X-ray diffraction evidence for the extensibility of actin and myosin filaments during muscle contraction. Biophys. J. 67:2422-2435.
9. Duke, T. 2000. Cooperativity of myosin molecules through strain-dependent chemistry. Phil. Trans. Roy. Soc. B355:529-538.
10. Higuchi, H., T. Yanagida, and Y.E. Goldman. 1995. Compliance of thin filaments in skinned fibers of rabbit skeletal muscle. Biophys. J. 69:1000-1010.

11. Griffiths, P.J., M.A. Bagni, B. Colombini, H. Amenitsch, S. Bernstorff, S. Funari, C.C. Ashley, and G. Cecchi. 2006. Effects of the number of actin-bound S1 and axial force on X-ray patterns of intact skeletal muscle. Biophys. J. 90:975-984.
12. Edman, K.A.P. 2009. Non-linear myofilament elasticity in frog intact muscle fibres. J. Exp. Biol. 212, 1115-1119.
13. Irving, T., Y. Wu, T. Bekyarova, G.P. Farman, N. Fukuda, and H. Granzier. 2011. Thick-filament strain and interfilament spacing in passive muscle: effect of titin-based passive tension. Biophys. J. 100:1499-1508.
14. Nocella, M., M.A. Bagni, G. Cecchi, and B. Colombini. 2013. Mechanism of force enhancement during stretching of skeletal muscle fibres investigated by high time-resolved stiffness measurements. J. Muscle Res. Cell Motil. 34:71-81.
15. Press, W.H., S.A. Teukolsky, W.T. Vetterling, and B.P. Flannery. 1992. Numerical Recipes in C. second edition, Cambridge University Press.
16. Brunello, E., M. Reconditi, R. Elangovan, M. Linari, Y-B. Sun, T. Narayanan, P. Panine, G. Piazzesi, M. Irving, and V. Lombardi. 2007. Skeletal muscle resists stretch by rapid binding of the second motor domain of myosin to actin. Proc. Natl. Acad. Sci. USA. 104, 20114-20119.
17. Fusi, L., M. Reconditi, M. Linari, E. Brunello, R. Elangovan, V. Lombardi, and G. Piazzesi. 2007. The mechanism of the resistance to stretch of isometrically contracting single muscle fibres. J. Physiol. 588, 495-510.
18. Lewalle, A., W. Steffen, O. Stevenson, Z. Ouyang, and J. Sleep. 2008. Single-molecule measurement of the stiffness of the rigor myosin head. Biophys. J. 94:2160-2169.
19. Kaya, M., and H. Higuchi. 2010. Nonlinear elasticity and an 8-nm working stroke of single myosin molecules in myofilaments. Science. 329:686-689.
20. Knight, P., and J. Trinick. 1984. Structure of the myosin projections on native thick filaments from vertebrate skeletal muscle. J. Mol. Biol. 177:461-482.
21. Ford, L.E., A.F. Huxley, and R.M. Simmons. 1977. Tension responses to sudden length change in stimulated frog muscle fibres near slack length. J. Physiol. 269:441-515.
22. Edman, K.A.P., G. Elzinga, and M.I.M. Noble. 1982. Residual force enhancement after stretch of contracting frog single muscle fibres. J. Gen. Physiol. 80:769-784.
23. Bagni, M. A., G. Cecchi, F. Colomo, and P. Garzella. 1994. Development of stiffness precedes cross-bridge attachment during the early tension rise in single frog muscle fibres. J. Physiol. 481:273–278.
24. Pinniger, G.J., K.W. Ranatunga, and G.W. Offer. 2006. Crossbridge and non-crossbridge contributions to tension in lengthening rat muscle: force-induced reversal of the power stroke. J. Physiol. 573:627-643.
25. White, H.D., and E.W. Taylor. 1976. Energetics and mechanism of actomyosin adenosine triphosphatase. Biochemistry. 15:5818-5826.13.
26. Ferenczi, M.A., E. Homsher, R.M. Simmons, and D.R. Trentham. 1978. Reaction mechanism of the magnesium ion-dependent adenosine triphosphatase of frog muscle myosin and subfragment 1. Biochem. J. 171:165-175.
27. Siemankowski, R.F., M.O. Wiseman, and H.D. White. 1985. ADP dissociation from actomyosin subfragment 1 is sufficiently slow to limit the unloaded shortening velocity in vertebrate muscle. Proc. Natl. Acad. Sci. USA. 82:658-662.
28. Huxley, A.F., and S. Tideswell. 1996. Filament compliance and tension transients in muscle. J. Muscle Res. Cell Motil. 17:507-511.
29. Decostre, V., P. Bianco, V. Lombardi, and G. Piazzesi. 2005. Effect of temperature on the working stroke of muscle myosin. Proc. Natl. Acad. Sci. USA. 102:13927-13932.
30. Offer, G., and K.W. Ranatunga. 2010. Crossbridge and filament compliance: implications for tension generation and lever arm swing. J. Muscle Res. Cell Motil. 31:245-265.
31. Nishizaka, T., R. Seo, H. Tadakuma, K. Kinosita, and S. Ishiwata 2000. Characterisation of single actomyosin rigor bonds: load dependence of lifetime and mechanical properties. Biophys. J. 79:962-974.

32. Piazzesi, G., M. Reconditi, N. Koubassova, V. Decostre, M. Linari, L. Lucii, and V. Lombardi. 2003. Temperature dependence of the force-generating process in single fibres from frog skeletal muscle. J. Physiol. 549:93-106.
33. Seebohm, B., F. Martinbehr, J. Kohler, A. Francino, F. Navarro-Lopez, A. Perrot, C. Ozcelik, W.J. McKenna, B. Brenner, and T. Kraft. 2009. Cardiomyopathy mutations reveal variable region of myosin converter as major element of cross-bridge compliance. Biophys. J. 97:806-824.
34. Reconditi, M., M. Linari, L. Lucii, A. Stewart, Y-B. Sun, P. Boesecke, T. Narayanan, R.F. Fischetti, T. Irving, G. Piazzesi, M. Irving, and V. Lombardi. 2004. The myosin motor in muscle generates a smaller and slower working stroke at higher load. Nature. 428:578-581.
35. Piazzesi, G., M. Reconditi, M. Linari, L. Lucii, P. Bianco, E. Brunello, V. Decostre. A. Stewart, D. B. Gore, T.C. Irving, M. Irving, and V. Lombardi. 2007. Skeletal muscle performance determined by modulation of number of myosin motors rather than motor force or stroke size. Cell. 131:784-795.
36. Huxley, H.E. 2006. X-ray interference studies of crossbridge action in muscle contraction: evidence from quick releases. J. Mol. Biol. 363:743-761.
37. Huxley, H.E. 2006. J. Mol. Biol. X-ray interference studies of crossbridge action in muscle contraction: evidence from muscle during steady shortening. J. Mol. Biol. 363:762-772.
38. Lombardi, V., G. Piazzesi, and M. Linari. 1992. Rapid regeneration of the actin-myosin power stroke in contracting muscle. Nature. 355:638-641.
39. Irving, M., V. Lombardi, G. Piazzesi, and M.A. Ferenczi. 1992. Myosin head movements are synchronous with the elementary force-generating process in muscle. Nature. 357:156-158.
40. Piazzesi, G., and V. Lombardi. 1995. A cross-bridge model that is able to explain mechanical and energetic properties of shortening muscle. Biophys. J. 68:1966-1979.
41. Chen, Y-D., and B. Brenner. 1993. On the regeneration of the actin-myosin power stroke in contracting muscle. Proc. Natl. Acad. Sci. USA. 90:5148-5152.
42. Linari, M. and R.C. Woledge. 1995. Comparison of energy output during ramp and staircase shortening in frog muscle fibres. J. Physiol. 487:699-710.
43. Piazzesi, G., and V. Lombardi. 1996. Simulation of the rapid regeneration of the actin-myosin working stroke with a tight coupling model of muscle contraction. J. Muscle Res. Cell Motil. 17:43-53.
44. Higuchi, H., and Y. Goldman 1991. Sliding distance between actin and myosin filaments per ATP molecule hydrolysed in skinned muscle fibres. Nature. 352:352-354.
45. Howard, J. 2001. Mechanics of motor proteins and the cytoskeleton. Sinauer Associates.
46. Cecchi, G., P.J. Griffiths, and S.R. Taylor. 1982. Muscular contraction: kinetics of crossbridge attachment studied by high-frequency stiffness measurements. Science, 217:70-72.
47. Cecchi, G., P.J. Griffiths, and S. Taylor. 1986. Stiffness and force in activated frog skeletal muscle fibers. Biophys. J, 49:437-451.
48. Ford, L.E., A.F. Huxley, and R.M. Simmons. 1986. Tension transients during the rise of tetanic tension in frog muscle fibres. J. Physiol. 372:595-609.
49. Lombardi, V. and G. Piazzesi. 1990. The contractile response during steady lengthening of stimulated frog muscle fibres. J. Physiol. 431:141-171.
50. Eisenberg, E., T.L. Hill, and Y-D. Chen. 1980. Cross-bridge model of muscle contraction. Quantitative Analysis. Biophys. J. 29:195-227.
51. Pate, E., and R. Cooke. 1989. A model for crossbridge action: the effects of ATP, ADP and Pi. J. Muscle Res. Cell Motil. 10:181-196.
52. Edman, K.P., A. Månsson, and C. Caputo. 1997. The biphasic force-velocity relationship in frog muscle fibres and its evaluation in terms of cross-bridge function. J. Physiol. 503:141-156.
53. Duke, T.A.J. 1999. Molecular model of muscle contraction. Proc. Natl. Acad. Sci. USA.

96:2770-2775.
54. Smith, D.A., and S.M. Mijailovich. 2008. Towards a unified theory of muscle contraction. II. Predictions with the mean-field approximation. Ann. Biomed. Eng. 36:1353-1371.
55. Månsson, A. 2010. Actomyosin-ADP states, interhead cooperativity, and the force-velocity relation of skeletal muscle. Biophys. J. 98:1237-1246.

(a) models with one tensing step

limit	$k_a'^{AM}$ s^{-1}	k_d^{AM} s^{-1}	k_{hyd} s^{-1}	k_{-hyd} s^{-1}	K_{tens}^{AM}	k_{tens}^{AM} s^{-1}	k_i^{AM} s^{-1}	Δ_D nm	κ pN/nm	l nm	d nm	f	c
lower	10	0.1	20	4	25	450	50	0.3	0.4	5	0.25	0.0	0.1
upper	1500	400	100	20	10000	50000	20000	10	3.5	13	5.0	1.0	1.0

(b) models with two tensing steps

limit	$k_a'^{AM}$ s^{-1}	k_d^{AM} s^{-1}	k_{hyd} s^{-1}	k_{-hyd} s^{-1}	K_{tens1}^{AM}	K_{tens2}^{AM}	k_{tens1}^{AM} s^{-1}	k_{tens2}^{AM} s^{-1}	k_i^{AM} s^{-1}	Δ_D nm	κ pN/nm	l_1 nm	l_2 nm	d nm	f_1	f_2	c
lower	10	0.1	20	4	4.5	5	200	250	50	0.3	0.5	0	0	0.25	0	0	0.1
upper	1500	400	100	20	1000	2500	50000	50000	18000	10	3.5	10	10	4.0	1.0	1.0	1.0

Table S1 Lower and upper limits of parameters used in final stage of refining models

Model	muscle	states	attached conform-ations	tensing steps	steps affected by strain	effect of strain on rate constants	lengthening tension borne by	sites on actin filament binding heads	crossbridge stiffness (pN/nm)	filament compliance	fit to force-velocity relation	tension transients after length steps	optimum efficiency
Eisenberg, Hill & Chen (50)	Frog muscle at 1°C	4	2	1 Stroke distance 8 nm.	All steps involving attached heads.	Empirical	n.c.	Target area of 1 subunit every 36 nm.	-	None.	shortening limb only.	Fitting of dependence on length step of T_1, T_2 and rate of tension recovery.	Thermo-dynamic effficiency 55%.
Pate & Cooke (51)	Rabbit psoas 10°C	5	3	1 Stroke distance 7.5 nm.	All steps involving attached heads.	Empirical	n.c.	Linear array of subunits 5.4 nm apart?	2.1	None.	shortening limb only.	n.c.	Mec.hanical efficiency >50% at < v_{max}/20.
Piazzesi & Lombardi (40)	Frog anterior tibialis	Total of 5 states in two cyclic pathways.	3	2 Stroke distances both 4.5 nm. Detachment & rapid reattachment can occur after first.	All steps involving attached heads.	Empirical	n.c.	Only one subunit along linear array.	0.7	None.	shortening limb only.	Fitting of dependence on length step of T_1, T_2 and rate of tension recovery	Mechanical efficiency 33% at ~v_{max}/5.
Smith & Geeves (4,5)	Rabbit psoas 20°C	6 reducible to 4.	2	1 Stroke distance 11 nm.	All steps involving attached heads except detachment of pre-tensing heads & reversal of tensing.	t.s.	Positively strained pre-tensing heads with ADP bound forcibly detached at high strain.	3 consecutive subunits 5.5 nm apart along linear array.	0.54	None.	shortening limb only.	n.c.	n.c.
Huxley & Tideswell (28)	Frog anterior tibialis ~2°C	4	3	2 Stroke distances 5.4 and 4.5 nm.	All steps involving attached heads.	t.s.	n.c.	5 consecutive subunits 5.5 nm apart along linear array.	2.0	Filament contribution to isometric sarcomere compliance 0.5.	Not shown.	Fitting of dependence on length step of T_1, T_2 and rate of tension recovery.	n.c.

Edman, Månsson & Caputo (52)	frog anterior tibialis ~2°C	4	3	2 Stroke distances both 5 nm.	All steps involving attached heads. Attachment/ detachment pre-tensing heads also velocity dependent.	Empirical	n.c.	Target area of 1 subunit per 37 nm.	1.5	None.	shortening limb only.	Qualitative fitting of T_1 & T_2 although not studied in detail.	n.c.
Duke (53)	Frog anterior tibialis 2°C	6 reducible to 3.	3	2 Stroke distance ~11 nm for first, 0.5 nm for second.	All steps involving attached heads except detachment of pre-tensing heads.	t.s.	Positively strained pre-tensing heads with ADP+Pi bound.	Continuous	1.3	None.	shortening, and for small lengthening velocities.	n.c. for isometric.	Mechanical efficiency 45% (~31% thermo-dynamic efficiency).
Smith & Mijailovich (54)	Frog anterior tibialis	9	3	2 Stroke distances both 4.5nm & both coupled to Pi release.	All steps involving attached heads except Pi release.	t.s	Heads after first tensing step with ADP bound, forcibly detached at high strain.	Target area 3 subunits per 36 nm.	1.7	Filament contribution to isometric sarcomere compliance 0.564.	shortening limb.	Fitting of T_1 & T_2 for releases only.	Mechanical efficiency 60% (~41% thermo-dynamic efficiency).
Månsson (55)	Frog anterior tibialis	7 reducible to 4	3	2 First stroke distance (6 nm), second (1 nm) on isomerisation of AM.ADP	All steps involving attached heads.	Empirical	Not explicitly stated	Target area of 1 subunit per 36 nm.	2.8	Mainly not considered.	shortening limb, & of lengthening limb	Qualitative fitting of T_1 & T_2	Thermo-dynamic efficiency 39%.
current paper	Frog anterior tibialis	5	3	2 Stroke distances (5.7 and 4.5 nm).	All steps involving attached states.	t.s.	Pre-tensing heads with ADP+Pi bound. Detachment rate increases monotonically with strain.	Target area of 3 subunits per 36 nm.	1.7	Filament contribution to isometric sarcomere compliance 0.533.	shortening & lengthening limbs.	Fitting of T_1 & T_2 for releases & stretch.	Thermo-dynamic efficiency 35%

Table S2. Comparison of mechano-kinetic models of the crossbridge cycle that have been used to fit muscle mechanics data.
n.c. not considered
t.s. rate constants calculated by transition state theory

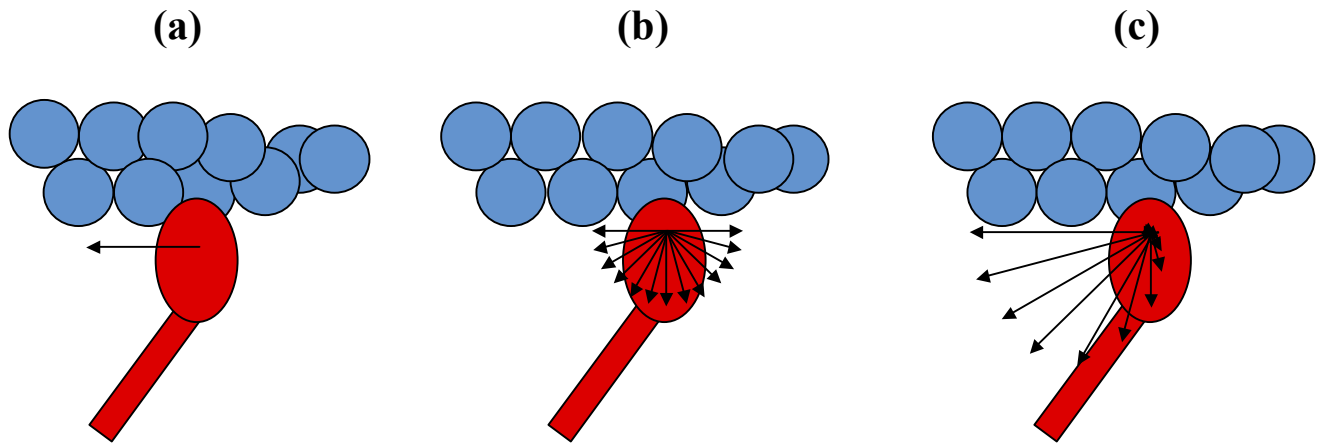

Fig. S1 Cartoon illustrating two possible modes of detachment of pre-tensing heads from actin.
(a) polar mode (b) symmetric mode in solution (c) symmetric mode in muscle. The myosin motor domain is depicted by a red ellipse, the lever arm by a red rectangle and actin subunits by blue circles. The arrows indicate the direction of the detachment along which the myosin head can detach in each mode, their relative length indicating the relative magnitudes of the rate constant for detachment at x=2 nm.

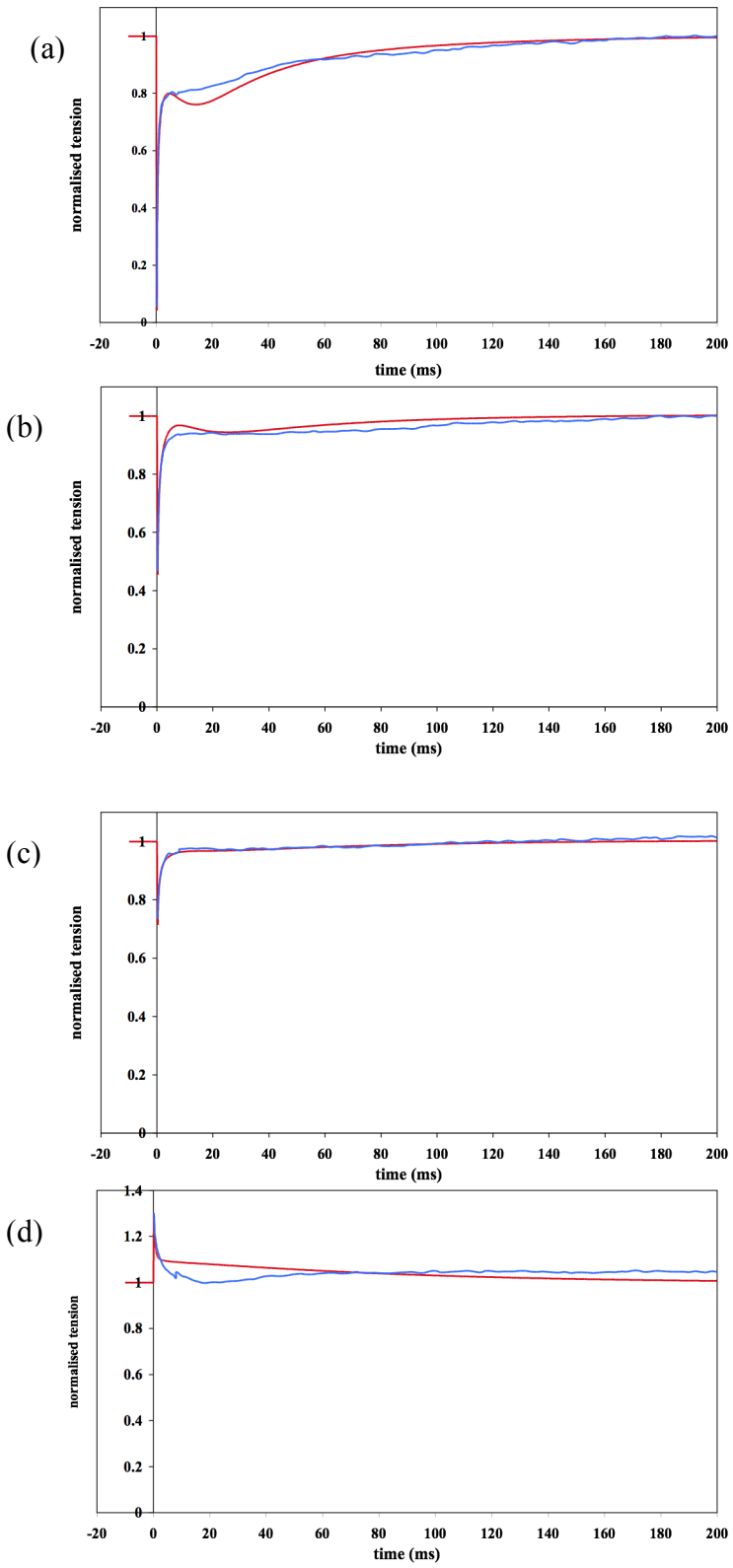

Fig. S2 Comparison with experimental data of long time courses of tension transients after rapid length steps for model with two tensing steps.
Experimental data of Ford et. al. (21) (blue line), response of model (red line). Releases of a) 6 nm/hs b) 3 nm/hs c) 1.5 nm/hs and d) a stretch of 1.5 nm/hs.

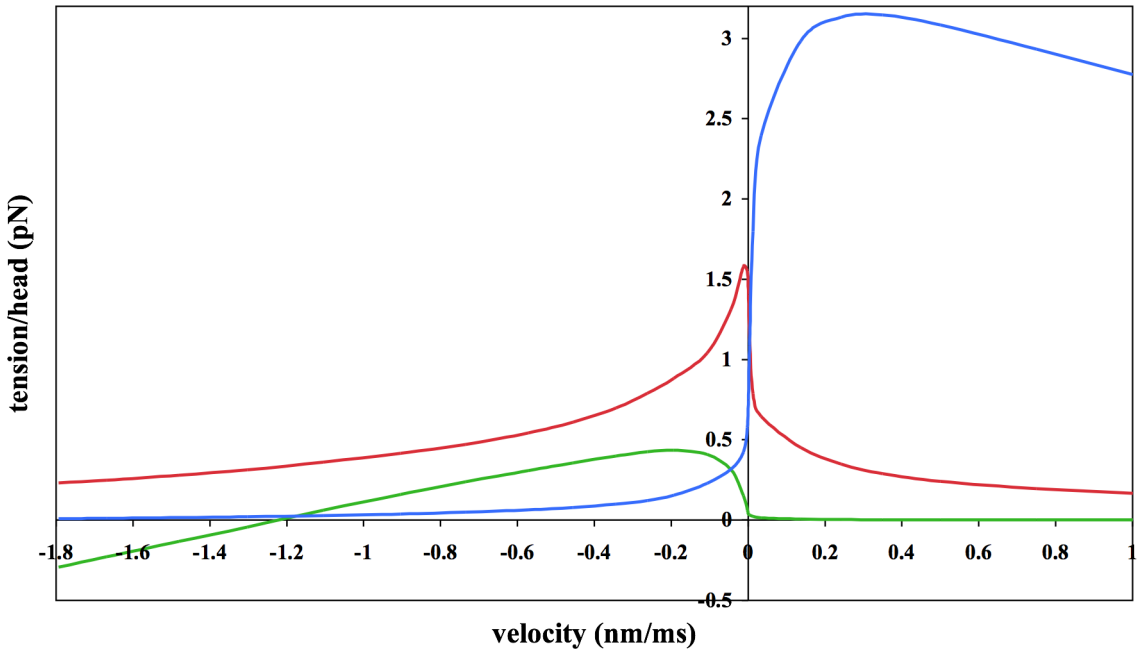

Figure S3 Velocity dependence of tension contributions of attached states.
pre-tensing heads blue, mid-tensing heads red, post-tensing heads green.

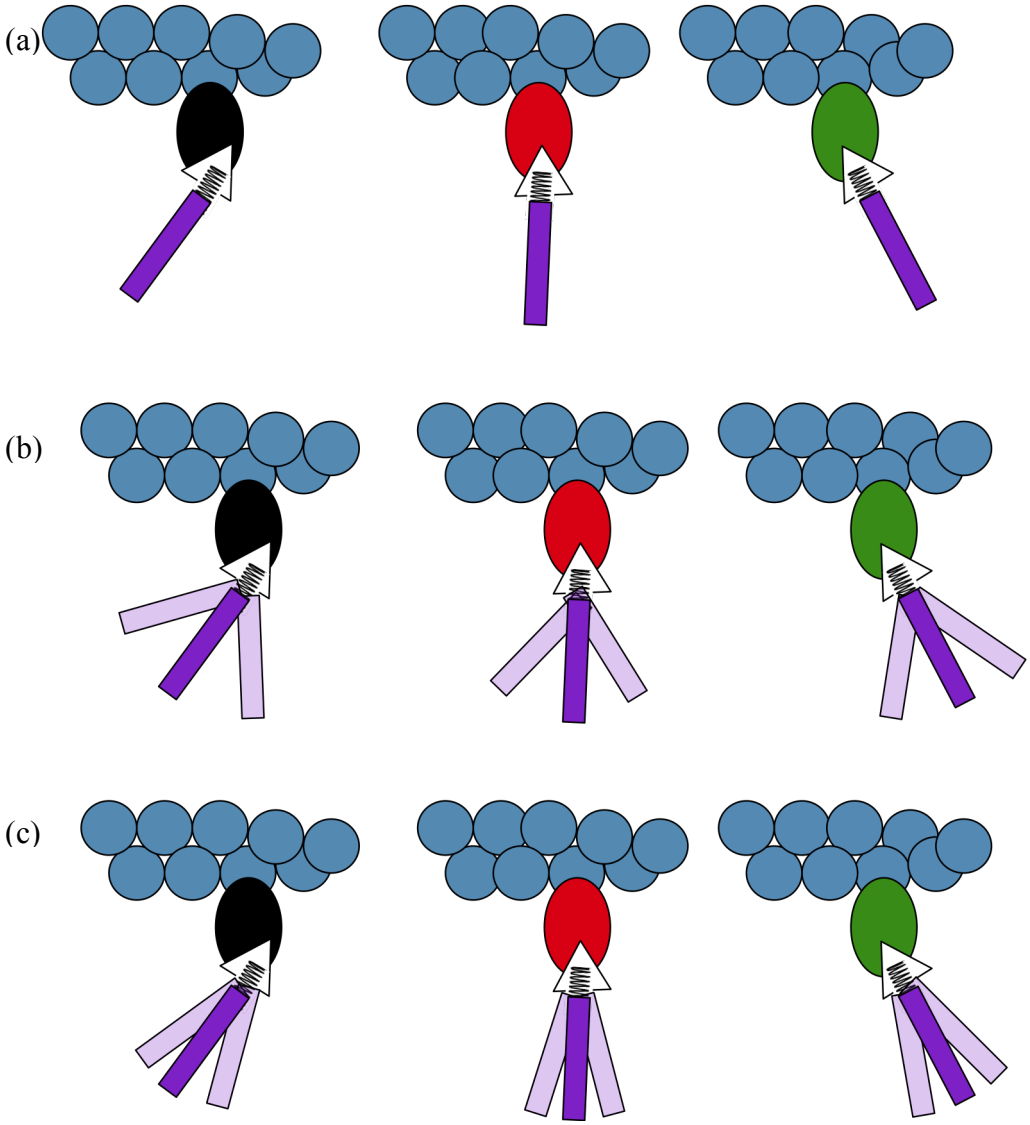

Fig. S4 Cartoons illustrating the difference between high and low cooperativity mechanisms.
(a) to (c) illustrate how lever arm angle is affected by motor domain conformation and by crossbridge stiffness.
(a) The orientation of the converter domain and the unstrained lever arm angle are determined by the conformation of the myosin head.
(b) With a low crossbridge stiffness the lever arm can flex substantially on either side of the unstrained angle.
(c) For a high crossbridge stiffness the lever arm can flex only a little on either side of the unstrained angle.
Actin subunits are represented by blue circles, the motor domains of myosin heads by ellipses (the change in colour from black to red to green indicates a change in conformation). The converter subdomain is represented by a white triangle, the lever arm by a purple rectangle, and the compliant element between them by a spring.

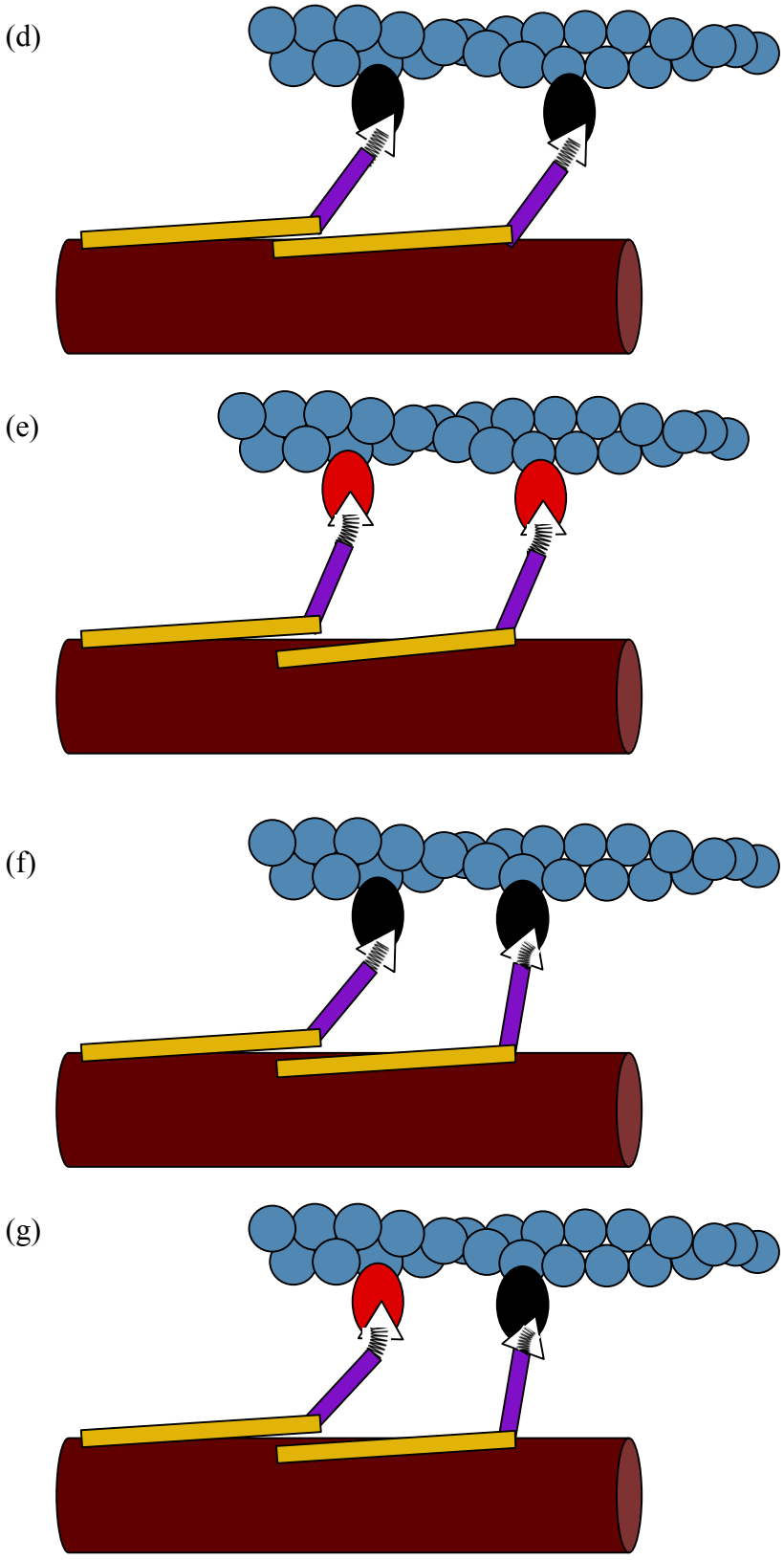

Fig S4 continued.
If the crossbridge stiffness is high (d) pre-stroke heads attach with similar lever arm angles and (e) after a length step synchronously change conformation and lever arm angle.

Low crossbridge stiffness allows (f) pre-stroke heads to attach with a range of lever arm angles and (g) develop isometric tension by a minority changing conformation without filament sliding.
Brown cylinder thick filament backbone, yellow rectangles subfragment-2 .

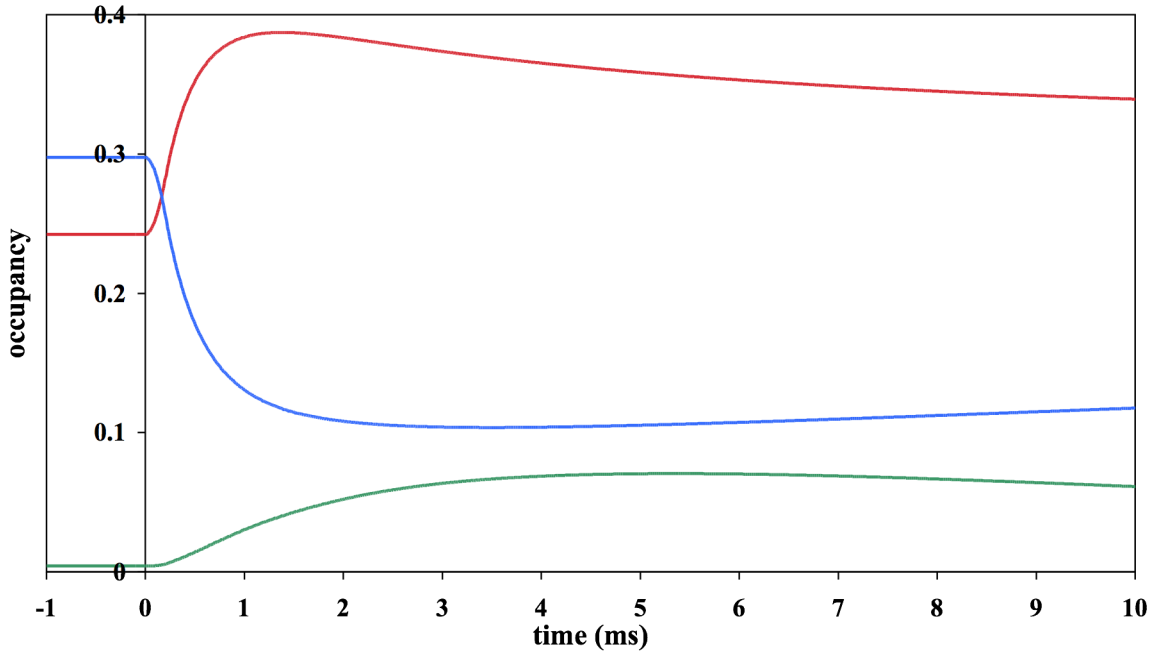

Figure S5 The time course of the occupancies of attached states in response to a length release of 3 nm/hs in 0.2 ms.
Occupancy of pre-tensing heads blue, mid-tensing heads red, post-tensing heads green.

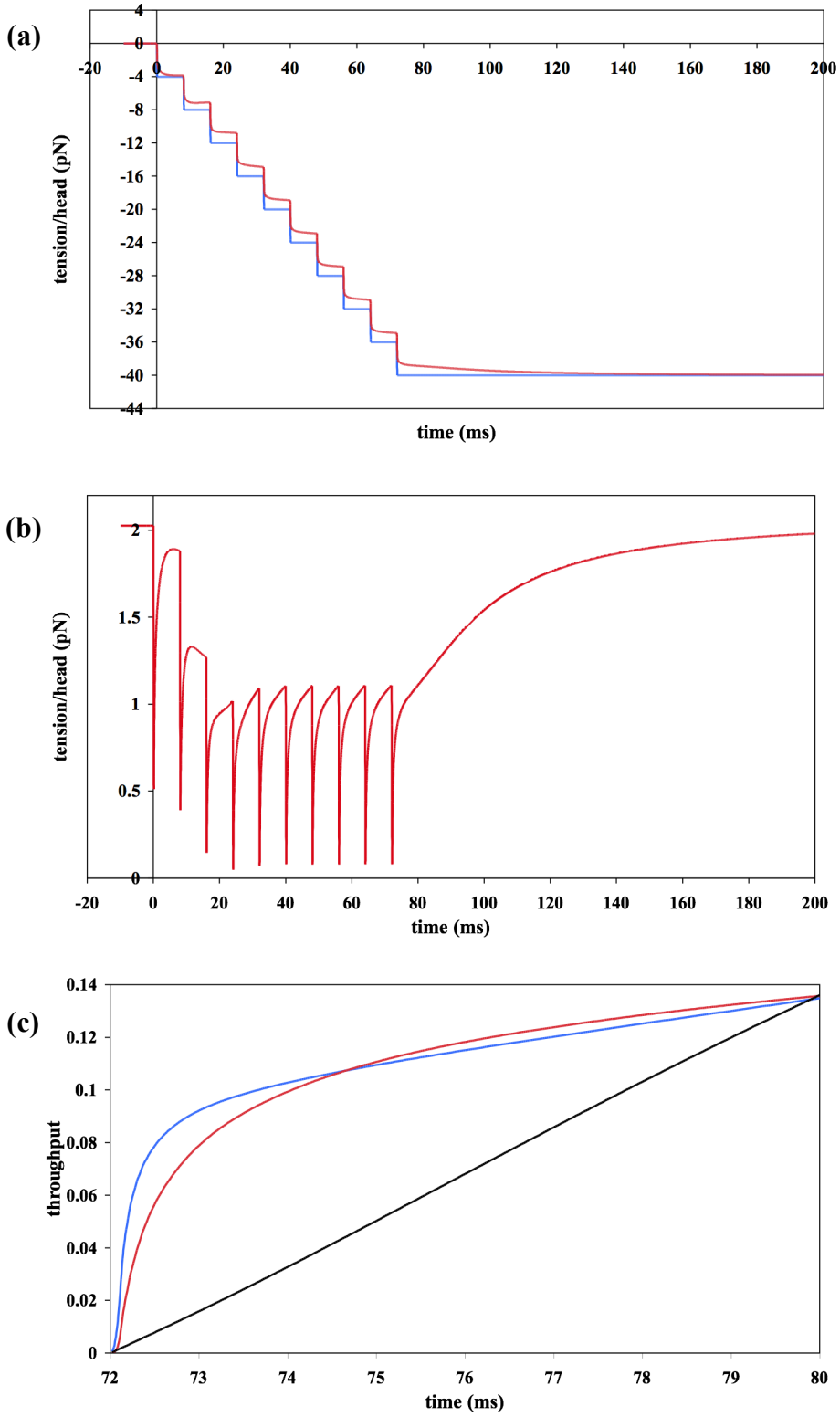

Fig. S6 Simulation of staircase shortening by model.
The simulation shows the response to ten releases of 4 nm/hs each in 0.11 ms repeated every 8 ms. Time courses of (a) the change in half-sarcomere length (blue) and length slid by filaments (red) (b) the resulting tension transients (c) the throughput of heads through the first tensing step (blue), the second tensing step (red) and the hydrolysis step (black) in the last repeat.

(a)

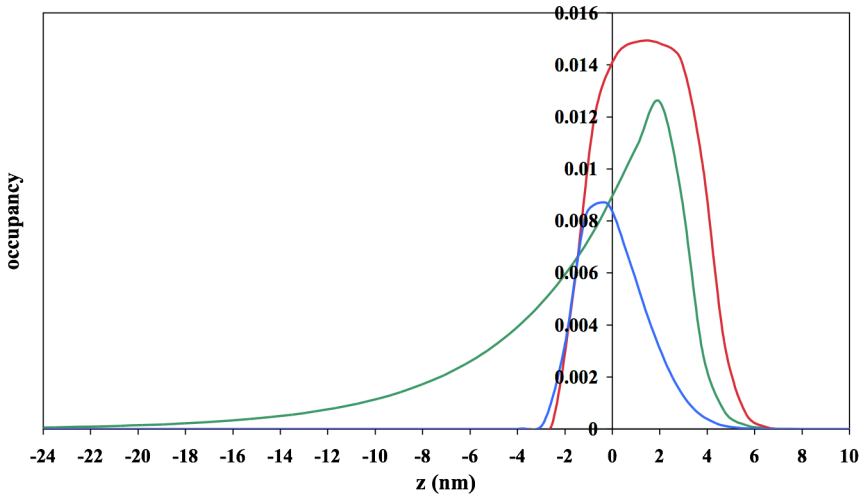

(b)

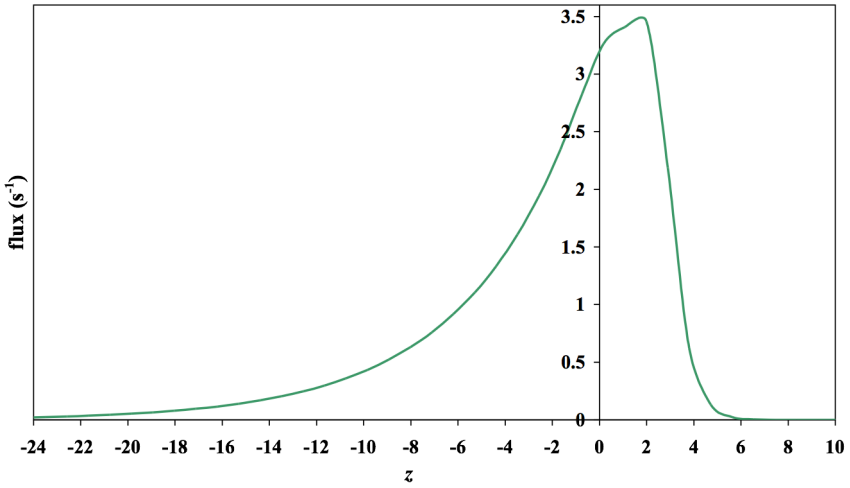

Fig S7. Strain distribution of occupancies of attached states and of flux for detachment
(a) *z* distribution of occupancies of pre-tensing heads (blue), mid-tensing heads (red) and post-tensing heads (green).
(b) z distribution of flux of detachment from post-tensing heads.

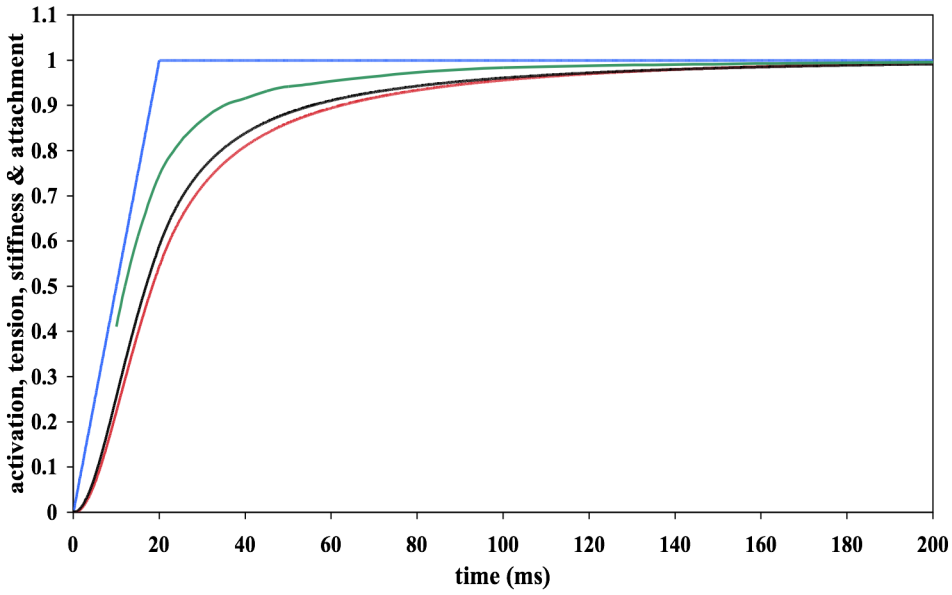

Fig. S8 Time course of stiffness, attachment and tension during activation.
Assumed time course of activation of thin filament (blue), stiffness (green), occupancy of attached heads (black), tension (red) all relative to final values.

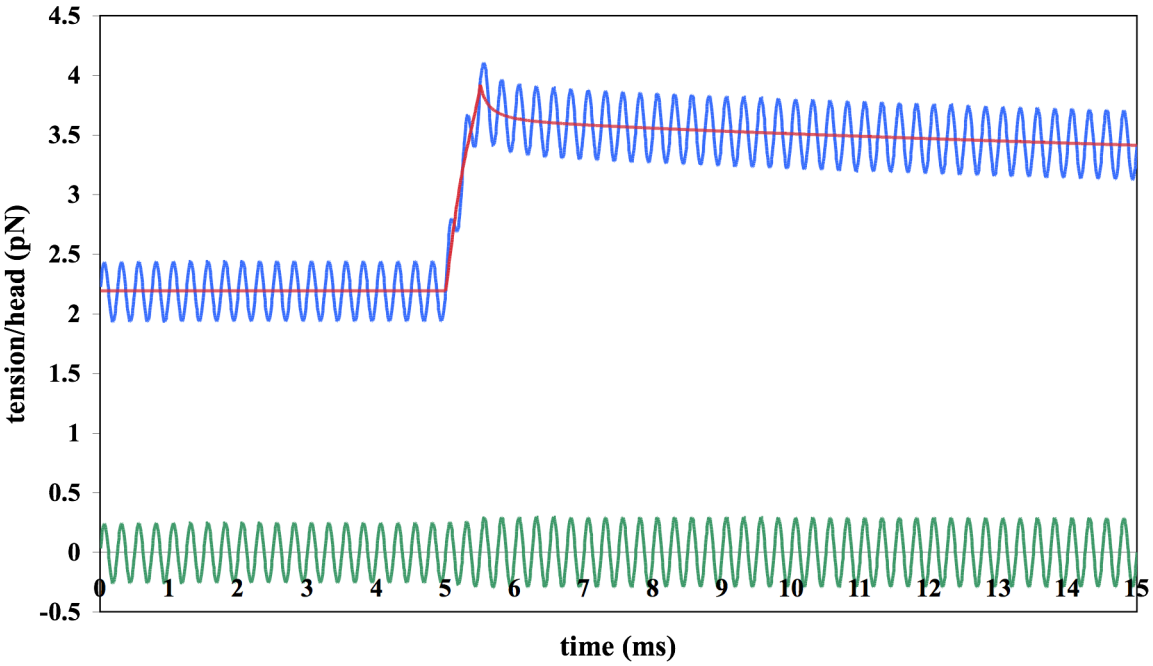

Fig. S9 Time course of tension in response to stretch of 5 nm/hs in 0.5 ms at 5 ms. With superposed 4 Hz oscillation (blue), without oscillation (red) and tension difference between them (green).

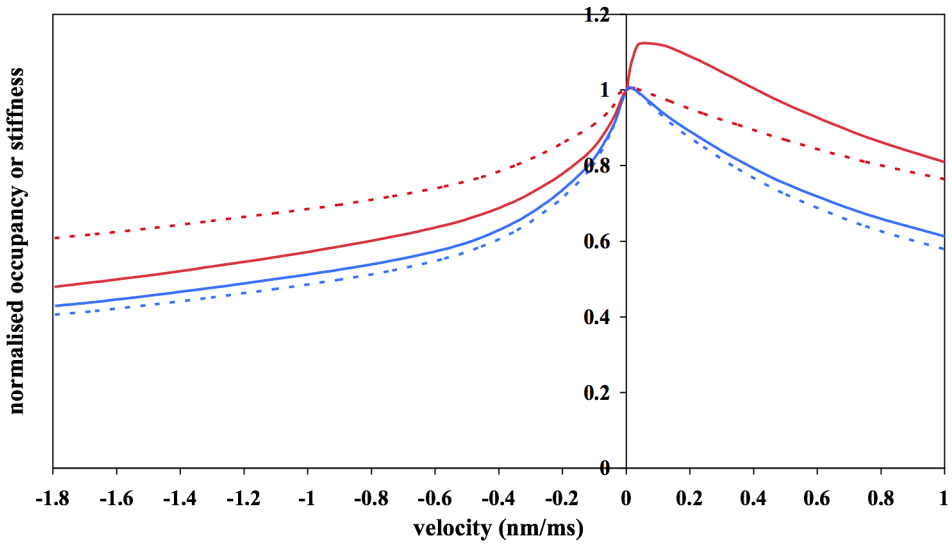

Fig. S10 Comparison of velocity dependence of occupancy of attached heads & stiffness for current non-Hookean model and precursor Hookean model
Full lines non-Hookean model, dashed lines previous Hookean model. Occupancy of attached heads (blue), stiffness (red) both relative to isometric value.